Simplifying Asynchronous Optical Sampling: A New Experimental Approach Toward Industrial Integration exploiting Lock-in acquisition

SIMONE PELI,[1] ANDREA TOGNAZZI,[2,3,*], PAOLO FRANCESCHINI,[3,4], MARCO GANDOLFI,[3,4], CLAUDIO GIANNETTI,[3,5], GABRIELE FERRINI,[5], AND FRANCESCO BANFI[6]

[1]*Castellini Officine Meccaniche, Via Privata Giuseppe Castellini 2, Cazzago San Martino, 25046, Italy*
[2]*Dipartimento di Ingegneria, Università degli Studi di Palermo, Viale delle Scienze ed. 10, Palermo, 90128, Italy*
[3]*Istituto Nazionale di Ottica - Consiglio Nazionale delle Ricerche (INO-CNR), Via Branze 45, Brescia, 25123, Italy*
[4]*Dipartimento di Ingegneria dell'Informazione, Università degli Studi di Brescia, Via Branze 38, Brescia, 25123, Italy*
[5]*Interdisciplinary Laboratories for Advanced Materials Physics (I-LAMP) and Dipartimento di Matematica e Fisica, Università Cattolica del Sacro Cuore, Via Garzetta 48, Brescia, 25133, Italy*
[6]*FemtoNanoOptics group, CNRS, Université Claude Bernard Lyon1, Institut Lumière Matière, 69622 Villeurbanne, France*
[*]*andrea.tognazzi@unipa.it*

Abstract: Time-resolved optical spectroscopies are emerging as a go-to technique for non-destructive testing of nanomaterials. Inspecting the thermal and mechanical properties of a mesoscale device requires achieving delay times beyond the ns timescale in a nanoscopy setup, potentially in a vibration polluted environment. These requirements constitute a major challenge for traditional pump-probe techniques based on moving mechanical delay lines and Lock-in detection. ASynchronous Optical Sampling (ASOPS) and Electronically Controlled Optical Sampling (ECOPS), avoiding any moving mechanical part, are good alternatives. However, their detection scheme is based on fast-balanced photodiodes, which, as a technology, is not as wide-spread, not as developed and lacks the performance of Lock-in based detection. In this study, we introduce a novel approach that integrates ASOPS/ECOPS and Lock-in detection methodologies, eliminating the necessity for a reference signal and streamlining the optical configuration. By leveraging the strengths of each technique, our approach enhances simplicity and efficiency. The scheme is first validated against standard approaches in the frame of a beam-depletion measurement in a sum frequency experiment. It is then tested in a paradigmatic case study to inspect the mechanics of a single gold nanodisk, with dimensions in the 100 nm range, nanopatterned on a sapphire substrate. These results widen the range of applicability of time-resolved optical techniques as a nano-metrology tool to industrial settings.

1. Introduction

Ultrafast time-resolved optical spectroscopy, a consolidated technique in solid-state physics, is ramping up at a tremendous pace in fields ranging from nano-optics [1–8], nano-phononics [9–12], to bio-mechanics [13–15] and non-destructive thermo-mechanical nanometrology [16–27]. Concisely, the technique working principle is as follows [28]. A pump laser pulse impulsively excites the system varying its optical constants. A time-delayed, low-intensity, probe pulse measures the transient reflectivity/transmittivity changes as the system's relaxes back to equilibrium. The system's dynamical properties are ultimately encoded in the transient optical signal.

In its standard implementation, the technique relies on (a) Lock-in detection [28,29] of the probe beam (at the pump modulation frequency) via a single slow photo-detector and (b) controlling

the pump and probe temporal delay by changing the optical path of one the beams through a translating mechanical stage. Pros and cons of the standard implementation stand in points (a) and (b), respectively. Lock-in detection grants superior signal-to-noise ratio [29]. It relies on Lock-in amplifiers, that is a well-established, state-of-the art, relatively cheap technology, readily achievable in most optics lab. On the contrary, controlling the delay-time via a moving-stage may prove challenging in many situations such as: (i) when the relevant system dynamics extends to the ns timescale, since a tiny misalignment of the delay line mirrors affects the beams overlap; (ii) the pump and probe spot sizes are focused to the diffraction limit, *e.g.*, in microscopy applications; (iii) in situations where the setup mechanical stability is an issue, as might be the case in an industrial environment with external vibration sources. Indeed, in the above-mentioned scenarios, the main challenge is to maintain mutual alignment of the pump and probe beams, on top of the sample, over long travel ranges of the linear translation stage (1 ns delay-time corresponds to a 15 cm linear translation stage), while keeping the total acquisition time within reasonable boundaries. These issues arise for instance in the frame of thermo-mechanical nanometrology of single nano-objects and non-destructive inspection of meso-scale devices [30].

Among the proposed techniques to overcome these limitations [31], ASyncronous Optical Sampling (ASOPS) and its variant, Electronically Controlled Optical Sampling (ECOPS), stand out [32–34]. Both methods are based on two laser sources with synchronized repetition rates f_A and f_B, respectively. One laser provides the pump and the other the probe beam. A laser repetition rate is fixed by the cavity length. Detuning the two cavities by a small frequency amount Δf then allows controlling the delay between the pump and the probe pulses, avoiding any moving mechanical parts [35]. Because of this advantage ASOPS has been exploited to inspect the mechanics of single cells [36–38], nanoscale ultrasonic transducers [39], thin films [20, 40–42], polymers [43, 44], 2D van der Walls layers [45], phononic crystals [46, 47] and nanowires [48], nondestructive inspection of objects [49], all instances necessitating long delay times. However, ASOPS and ECOPS require a fast balanced photo-detector for signal acquisition and a fast digitizer acquisition board, which as a technology is not as wide-spread, not as developed and lack the performance of Lock-in based detection. Furthermore, the relative response of the two photo-diodes composing the balanced photo-detector may change during long acquisitions times, thus biasing the time-resolved signal.

We propose a scheme combining ASOPS and Lock-in detection, merging the pros of both techniques, that is Lock-in detection and asynchronous optical sampling. The manuscript is organized as follows. An overview of the time-resolved schemes is provided in Sec. 2, together with their comparison in Sec. 3. The ASOPS-Lock-in scheme is then presented in Sec. 4. The scheme is validated against the standard approaches in the frame of a beam depletion measurement in sum frequency generation, Sec. 5. The scheme is then successfully deployed to inspect the mechanics of a single gold nanodisk, with dimensions in the 100 nm range, nanopatterned on a substrate, Sec. 6. This scenario is particularly well suited to test the scheme since it involves accessing long-delay times in a nanoscopy setup. The case study is thus paradigmatic of situations where the approach is particularly apt.

2. Overview of time-resolved optical schemes

In an optical pump-probe experiment, the sample's excitation via an ultrashort laser pump pulse at time t_0 leads to a transient optical reflectivity, $R(t)$, and transmittivity, $T(t)$, of the material. A delayed lower intensity probe pulse is exploited to measure the reflectivity (transmittivity) variation $\Delta R(t)$=$R(t) - R_0$ ($\Delta T(t)$=$T(t) - T_0$) while the sample relaxes back to equilibrium, with R_0 (T_0) being the equilibrium reflectivity (transmittivity), *i.e.*, in the absence of pump excitation. By measuring R_0 (T_0) with the pump off then allows to obtain the relative transient reflectivity (transmittivity) $\Delta R/R_0$ ($\Delta T/T_0$). Here, we schematically review the implementation of the most common techniques.

2.1. Standard pump-probe

In the standard pump-probe technique, See Figure 1a), the train of pulses out of a single laser source is split into a pump and a probe beams. The time delay between the pump and the probe pulses is controlled varying their mutual path length via a sliding mechanical stage with maximum travel range L_{max}. The temporal resolution, $\Delta t = 2\Delta x/c$ (with c the speed of light), and the maximum time delay, $t_{max}^{stage} = 2L_{max}/c$, are determined by the linear stage minimum step size, Δx, and maximum traveling range, respectively. The train of pump pulses is modulated (via a chopper or photoacoustic modulator) at a reference angular frequency ω_{chop}, serving as reference for Lock-in detection. The probes intensity is recorded by a slow photodiode (PD) upon reflection/transmission from/through the sample. The PD output is fed to a Lock-in for detection at the reference angular frequency ω_{chop}. The Lock-in output is then fed to a computer, this procedure being repeated for each time-delay step. The Lock-in output is directly proportional to ΔR (ΔT). The longer the integration time of the Lock-in (during which the delay stage remains in a fixed position), t_I, the better the signal-to-noise ratio (S/N).

2.2. ASynchronous Optical Sampling (ASOPS)

The ASOPS technique [50] relies on two synchronized femtosecond lasers with stabilized repetition rates f_A (pump) and $f_B = f_A - \Delta f$ (probe), where the detuning Δf is such that $0 \leq \Delta f \ll f_A$. With reference to Fig. 2, let us assume that a pair of pump and probe pulses (pair 1: pulse A1 and B1, respectively) are spatially and temporally overlapped on the sample at time $t_0 = 0$. The next pump pulse strikes the sample at time $t_1 = 1/f_A$, whereas the next probe pulse strikes at time $t_1 + \Delta t = 1/(f_A - \Delta f)$. The accumulated time delay between this pair of pulses (pair 2: pulses A2 and B2) reads, upon Taylor's expansion, $\Delta t = \Delta f/f_A^2$. The time delay between the next pair of pump and probe pulses (pair 3: pulses A3 and B3) will be $2\Delta t$. The time delay $n\Delta t$ will keep increasing as the pair number n increases till a value n_{max}, where n_{max} is such that $n_{max}\Delta t = 1/f_A$, that is the pump and probe pulses are back in temporal coincidence. This occurs after a time span (in the laboratory time frame: lab time in Fig. 2) $n_{max} \times 1/f_A = 1/\Delta f$, whereas the sampled time delay window (delay time in Fig. 2) extends to $t_{max} = 1/f_A$. Summarizing, the repetition rate f_A sets the maximum delay time; the detuning Δf sets the time (in the laboratory frame) necessary to perform a complete time-delay scan; both f_A and Δf set the time-delay resolution, see Table 2.

The signal-to-noise ratio is improved acquiring and averaging multiple time-resolved traces, each one spanning the entire time-delay window. Let us call N_{scan} the number of averaged traces.

The layout for its practical implementation is schematically reported in Fig. 1b). A beam splitter (BS) splits the beam out of laser B in the actual probe and its reference beam. A fast balanced photodiode (bandwidth exceeding f_B), consisting in two fast photodiodes (PDs) and a fast differential amplifier, measures the difference between the intensity of the probe and reference beams after excitation of the sample by each pump pulse. The reference beam is conditioned, via an attenuator and a linear stage, so as to provide a zero output from the balance photo-detector when the sample is in equilibrium (pump beam turned off). The reference beam is conditioned once, before starting the measurements, the linear stage then remains fixed during the experiment, at variance with the standard pump-probe technique. The output from the balanced photodiode is then proportional to $\Delta R(t)$, if measuring in reflection, or $\Delta T(t)$, if measuring in transmission [51–53]. The balanced photodiode output is fed to a fast digitazing board connected to a computer.

2.3. Electronically Controlled Optical Sampling (ECOPS)

Eventually, the relaxation timescale of the phenomena under investigation may fall short of the maximal delay-time $1/f_A$ explored with ASOPS. In such instances, it is convenient to restrict the maximum time-delay window either to ameliorate the signal-to-noise level, by averaging

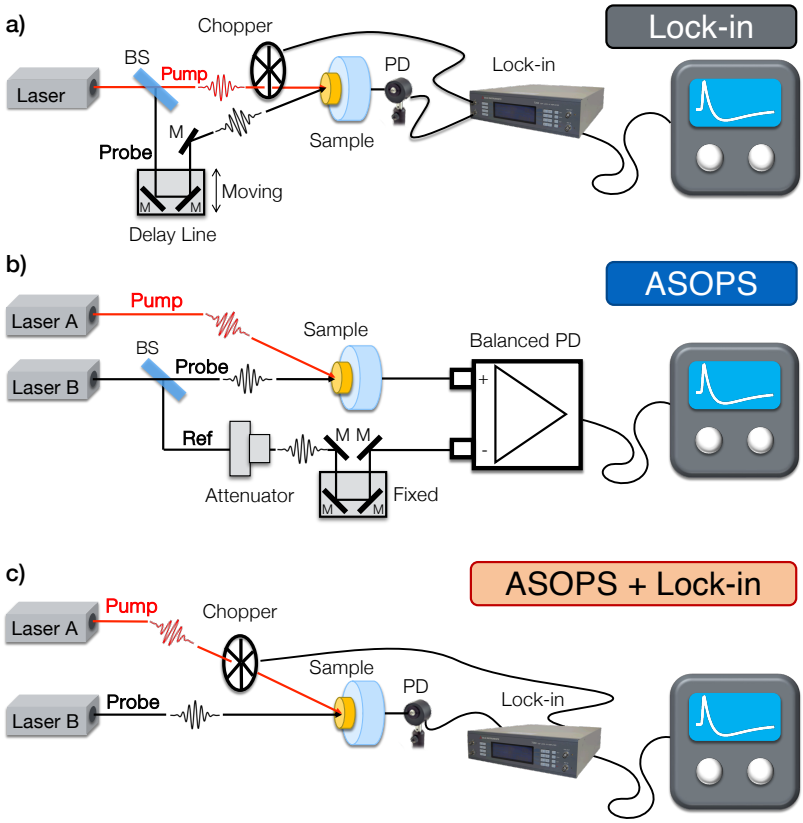

Fig. 1. Comparison among the three different setups addressed in the present work. PD: photo-detector; M: mirror; BS: beam splitter. a) Standard pump-probe technique. A BS splits the output of a single laser cavity in a pump and probe beam. The train of pump pulses is modulated by a chopper at a reference angular frequency ω_{chop}, serving as reference for Lock-in detection. b) Asynchronous OPtical Sampling (ASOPS) and Electronically Controlled Optical Sampling (ECOPS). They rely on two phase-stabilized optical combs, out of lasers A and B, providing the probe and pump beams. A BS splits the beam out of laser B in probe and reference beams. A fast balanced PD provides the difference between the intensity of the probe beam and its reference for each single pair of pump and probe pulses. c) ASOPS+Lock-in acquisition. The setup is greatly simplified and relies on: an ASOPS system; a slow PD; a chopper to modulate the pump beam and a Lock-in amplifier. Explanation in the text.

more scans within the same acquisition time, or reduce the acquisition time for the same S/N output. That is were the ECOPS variant to ASOPS comes handy. Similarly to ASOPS, also ECOPS exploits the frequency detuning between two laser cavities to control the pump-probe delay time. However, in ECOPS, the detuning Δf is switched from $|\Delta f|$ to $-|\Delta f|$ after a time interval $T_{sweep}/2$, see Fig. 3. Recall that $f_B = f_A - \Delta f$. Hence, when the detuning is set to $+|\Delta f|$, see step 1 in Fig. 3 top panel, the system works in the same way as ASOPS, *i.e.*, the probe delay time increases from $t_0 = 0$ to t_{max}, where now $t_{max} = (T_{sweep}/2)(|\Delta f|/f_A)$. At time $T_{sweep}/2$, step 4 in Fig. 3, the detuning is set to $-|\Delta f|$ and the probe time delay reverses direction, decreasing from t_{max} back to $t_0 = 0$. The Δf periodicity is T_{sweep}, and more periods are iterated to acquire multiple scans (two delay-time window scans, one forward and one backward, within each period T_{sweep}). Summarizing, T_{sweep}, f_A and Δf all set the maximum delay time; T_{sweep}

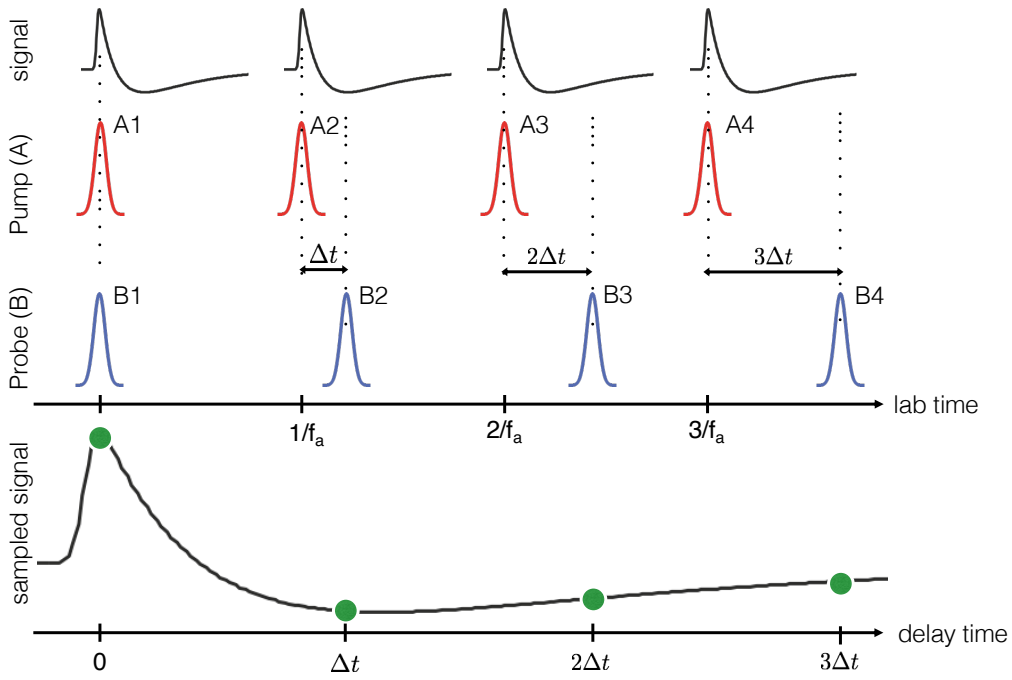

Fig. 2. ASOPS principle of operation. The repetition rate of laser A (pump) is f_A (second row: red pulses). The repetition rate of laser B (probe) is f_B (third row: blue pulses). Every $1/f_A$ seconds (lab time) the sample is excited in the same manner (second row: red pulses) and exhibits the same relaxation dynamics (first row: black curves). The first pair of pulses, A1-B1, are temporally (and spatially) coincident on the sample. Due to the frequency detuning Δf, in the second pair, the probe pulse probes the sample with a time-delay Δt (third raw: blue pulses) with respect to the pump-pulse (second row: red pulses). The time-delay increases linearly for each subsequent couple of pulses till it reaches the maximum delay $t_{max} = 1/f_A$. At that point, the temporal coincidence between the pump and the probe pulses is recovered and a second scan starts. The signal is reconstructed in the delay time frame (fourth row), where the delay time separating two subsequent points is Δt.

controls the time (in the laboratory frame) necessary to perform a complete time-delay scan; both f_A and Δf set the time-delay resolution (as for the ASOPS), see Table 2.

3. Comparing the techniques

In traditional pump-probe experiments, the probe signal is integrated at each time delay, while in ASOPS (ECOPS) multiple scans, acquired in a very short time, are averaged. The two parameters that control the number of measured probe pulses are the integration time to acquire multiple pulses at a fixed delay time for the standard technique and the number of scans for the ASOPS and ECOPS techniques. In order to compare the two techniques, the integration time (for the standard technique) and the number of scans (for the ASOPS technique) must be chosen so as to average the same number of pulses. In this particular configuration, the output of the experiment should be, theoretically, exactly the same.

However, laser fluctuations should be taken into account when comparing these techniques, since they affect the time-resolved trace differently. Lasers are subject to fluctuations of the output power for several reasons: temperature fluctuations of the room, humidity, vibrations etc.

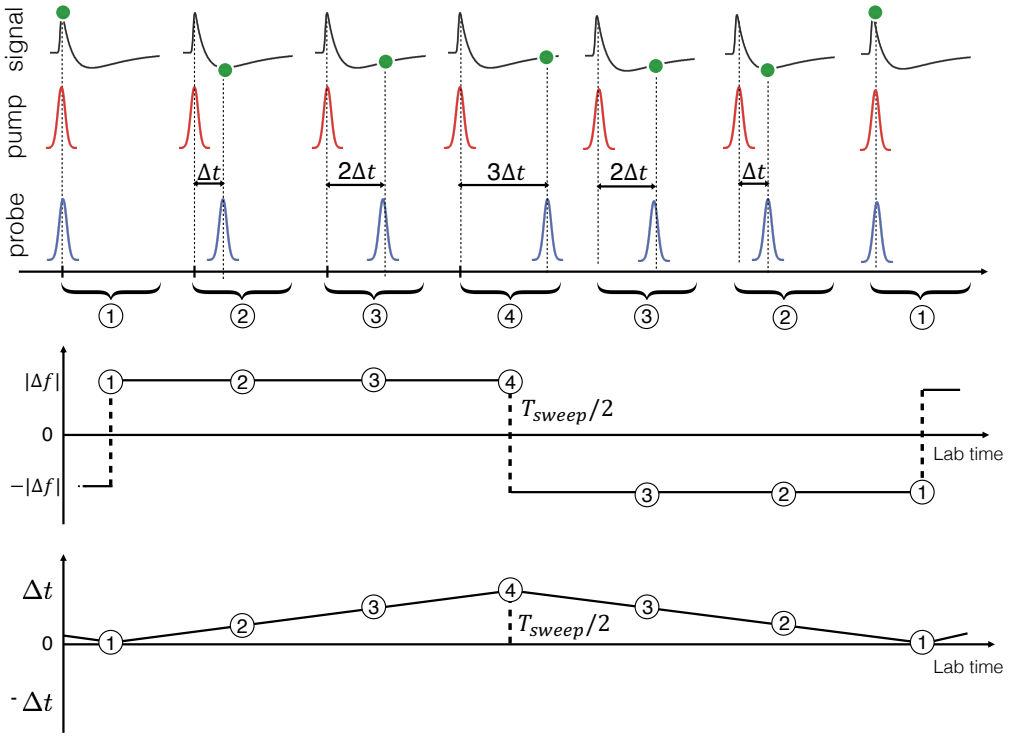

Fig. 3. ECOPS principle of operation. Step 1: pump and probe pulses are time (and space) coincident on the sample. Steps 1 to 4: the probe repetition rate is detuned by $\Delta f = |\Delta f|$ with respect to the pump. Recall that $f_B = f_A - \Delta f$, hence, in these steps $f_B \leq f_A$. The signal dynamics is measured at time-delays increasing by integer values of Δt. Step 4: at time $T_{sweep}/2$ (lab time) the detuning Δf is flipped to $-|\Delta f|$, hence, $f_B \geq f_A$. Steps 4 to 1: now the probe reduces its delay with respect to the pump and probes the signal backwards. In such a way, by flipping the detuning from $|\Delta f|$ to $-|\Delta f|$ and vice versa with periodicity T_{sweep}, only the desired delay time window is probed.

These fluctuations can affect the measurements significantly increasing the noise. In particular, in the standard pump-probe approach, due to the step-by-step nature of the acquisition scheme, the fluctuations of the laser intensity affects the data in different ways at different delay times. On the contrary, with the ASOPS and ECOPS, due to the very fast acquisition of a single scan over the whole delay window, the fluctuations affect equally the signal probed at all delay times within a single scan. Therefore, the artefacts due to the fluctuations are then averaged over the large number of scans measured. As a result, the effects of laser fluctuations are equally smeared over all delay times in ASOPS and ECOPS as opposed to traditional pump-probe.

4. Merging ASOPS and Lock-in Techniques

In this section, we introduce an innovative experimental approach consisting in merging ASOPS method with Lock-in detection (typical of the standard pump-probe). This enables to overcome the limitations due to misalignment of mechanical stages and expensive fast photo-detectors. To this end, we employ the experimental setup sketched in Fig. 1c. We underline that the same approach can be used to merge ECOPS with Lock-in detection, with the add-on of controlling the time delay window.

Table 1. **Pros and cons of traditional pump-probe, ASOPS and ECOPS.**

	Traditional pump-probe	ASOPS	ECOPS
Acquisition	Slow Lock-in detection	Fast balanced photo-detectors	
Maximum time delay	Limited by mechanical stage travel range (and laser repetition rate)	Fixed by laser repetition rate only	Tunable (up to a maximunm value limited by laser repetition rate)
Temporal resolution	Controlled by minimum mechanical stage step	Controlled by cavities detuning	
Noise reduction mechanism	Lock-in amplification	Average over multiple scans	
Single scan acquisition	Slowest	Intermediate	Fastest
Single scan noise	Low	High	
Laser fluctuations	Affect each time delay differently	Equally smeared over all delay times	

In this approach, the reference line is suppressed and the fast balanced photo-detector is replaced by a slow photo-detector connected to a Lock-in amplifier, which detects the probe intensity after the interaction with the sample. The two cavities are detuned by an amount $\Delta f > 0$ of the order of fractions of Hz (a value consistent with the specifications of the system). The instant at which the pump and probe pulses come in time-coincidence is used as a trigger for the asynchronous sampling and the data acquisition begins. This is achieved by an optical trigger (not shown in Fig. 1). Specifically, this instant can be determined with high temporal accuracy by feeding a small portion of the two beams on a Beta Barium Borate (BBO) crystal to generate a sum frequency signal (SFG). When the two pulses are in space and time-coincidence a sum frequency is generated and detected on a dedicated photodiode. The signal from the photodiode triggers the acquisition [50, 54]. As far as the acquisition system is concerned, the Lock-in amplifier necessitate a time interval t_I, *i.e.*, Lock-in integration time, measured in the frame of t_{lab}, to produce a single data point associated to a single delay time with an update rate $U_r = 1/t_I$. Therefore, as shown in Fig. 4, within a time interval t_I, the Lock-in records the signal delivered by a total number $N_p = t_I \cdot f_B \approx f_A/U_r$ of probe pulses. We note that, since $\Delta f \neq 0$ during asynchronous sampling, the total amount of time delay accumulated by N_p probe pulses is $d_p = N_p \cdot |\Delta t|$. This means that the physical information distributed over a time-delay interval d_p is enclosed in one single data point delivered by the Lock-in output. Since within t_I the Lock-in integrates N_p pulses, each corresponding to a different time-delay, the technique is sound provided that the physical feature of the sample that we are interested in changes on a time scale longer than d_p. Thus, the minimum delay time step for the optical trace is d_p.

Let us assume that the dynamics we are interested in yields optical changes on a time scale $\sim$ 100 fs. Hence, the probe pulses, whose time delay differ by less than 50 fs, have the same intensity. We thus target a d_p=50 fs. As a reference, we discuss the following example, which is achieved with a MenloSystem ASOPS system (see Sec. 5 for further technical details). In order to obtain d_p = 50 fs, given f_A = 100 MHz and t_I = 5 ms (U_r = 200 Hz), the detuning has to be set at Δf = 0.001 Hz (see summarizing Tab. 2). Given this value of the detuning, $\Delta t = 10^{-4}$ fs. Moreover, these setting choice implies that one single data point represents the average over

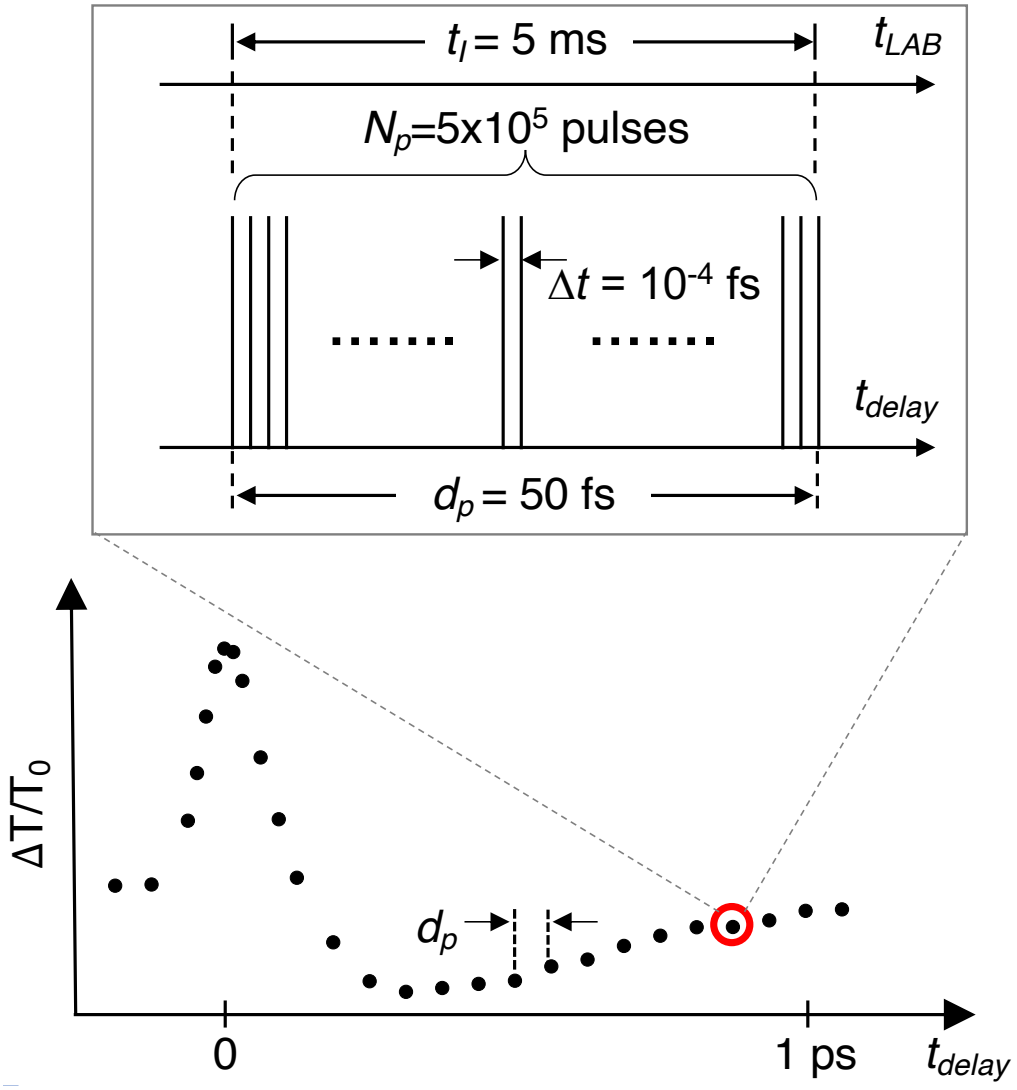

Fig. 4. Working principle of ASOPS+Lock-in technique. Time-resolved trace experimental data points are shown as black markers. Each data point provides the information on the dynamics at a given delay time t_{delay} value and it is obtained by averaging a number N_p of probe pulses (represented as black vertical segments in the inset). Since $\Delta f \neq 0$, a total time delay d_p is accumulated during the Lock-in integration time t_I. The reported numerical values correspond to the example discussed in the text.

$N_p = 5 \times 10^5$ probe pulses.

In Fig. 5, we compare the signal acquisition for the case of traditional Lock-in acquisition (left column), ASOPS (central column) and ASOPS+Lock-in method (right column). In traditional Lock-in detection, one fixes the time-delay and acquires the signal integrating for a time t_I. In the ASOPS method, the high S/N achieved at the end of the measurement is accomplished by averaging over many consecutive acquisitions of the entire time-resolved trace. On the other hand, in the ASOPS+Lock-in method, the overall trace is given by data points, each corresponding to the average of the probe signal over a time delay window d_p, with high S/N value. In this approach,

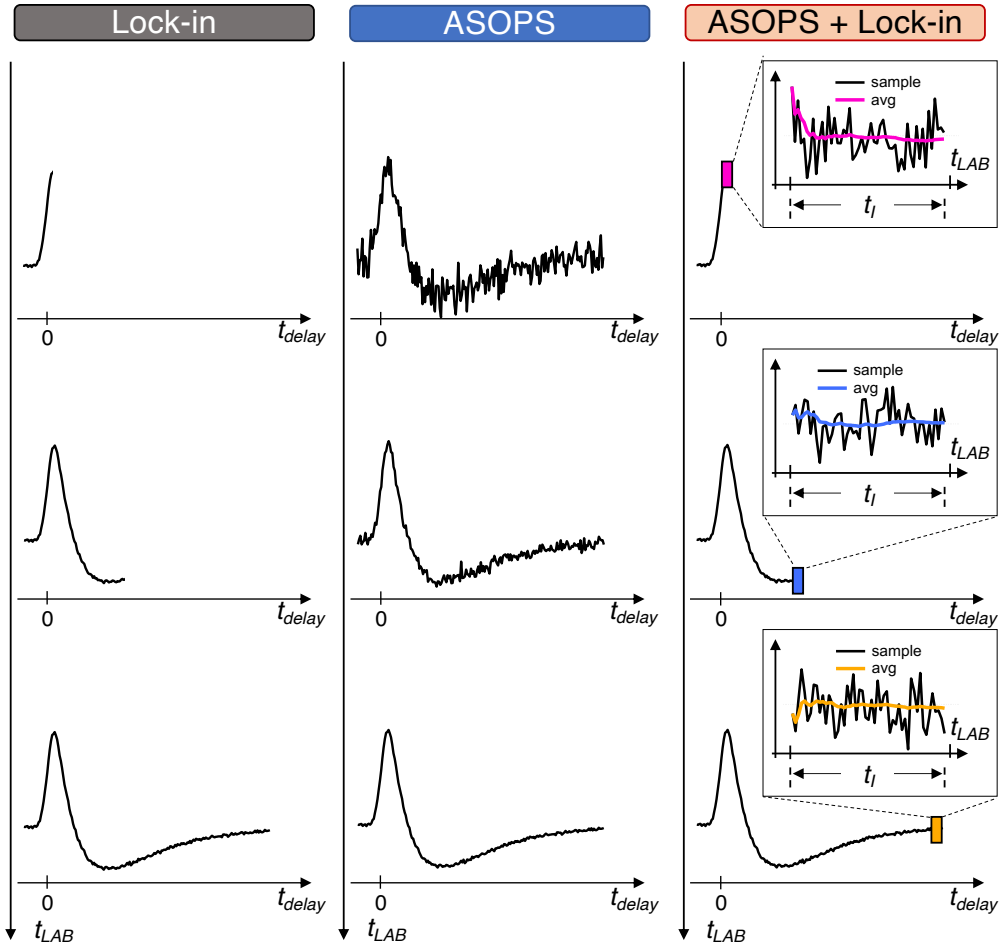

Fig. 5. Comparison between Lock-in, ASOPS, and ASOPS+Lock-in acquisition methods. The vertical axis (t_{LAB}) corresponds to the time in the laboratory frame and the horizontal axis to the delay time (t_{delay}). In each column, the bottom panel shows the measured trace as a function of t_{delay}. (Left) Lock-in acquisition. (Center) ASOPS acquisition. (Right) ASOPS+Lock-in acquisition. To increase the signal-to-noise ratio, the average over the signal from N_p pulses is performed (rectangular boxes), within a time interval t_I. The colored traces represent the average value of the points previously acquired in the time window. Refer to the main text for further explanations.

the S/N of each data point increases as a consequence of the averaging process performed within t_I.

5. Case Study

In this section, we present a case study to compare the capabilities of the proposed approaches, ASOPS+Lock-in and ECOPS+Lock-in, and compare them to those achieved by the standard ASOPS method.

Specifically, we analyze the beam-depletion in a SFG experiment [55]. Briefly, in SFG, the interaction within a nonlinear medium between two laser beams, at frequency ν_1 and ν_2, generates a third beam at frequency $\nu_3 = \nu_1 + \nu_2$, as sketched in the inset in Fig. 6a. As a

result, both the original pulses lose energy to populate a beam at frequency ν_3 due to energy conservation constrains. Two laser beams, delivered by a MenloSystem ASOPS Dual Color apparatus (Er:doped C-fiber lasers generating two trains of sub-150 fs pulses at $f_A = 100$ MHz), with pump $\nu_1 = 192.2$ THz ($\lambda_1 = 1560$ nm) and probe $\nu_2 = 384.4$ THz ($\lambda_2 = 780$ nm) frequency (wavelength), are focused on a type I BBO crystal, to generate a third beam at frequency (wavelength) $\nu_3 = 576.6$ THz ($\lambda_3 = 520$ nm). In the experiment, we monitor the variation of the transmitted intensity, $\Delta T(t)$, of the probe beam at $\nu_2 = 384.4$ THz and we report the normalized transmittivity variation $\Delta T(t)/T_0$ as a function of time, where t is the time-delay between the pump (at ν_1) and probe (at ν_2) pulses.

We employ three different techniques to measure $\Delta T(t)/T_0$: ASOPS, ASOPS+Lock-in and ECOPS+Lock-in. In this way we can compare the noise level, the acquisition time, and $\Delta T(t)/T_0$ resulting from the three different methods. We perform all measurements with the same beams parameters.

5.1. Case study: ASOPS measurement

The $\Delta T(t)/T_0$ trace recorded with the ASOPS setup is shown in Fig. 6a, b (red line). The detuning between pump and probe beams is set to Δf =500 Hz, which corresponds to a temporal resolution $\Delta t = 50$ fs. The time span of the time-delay window is $\Delta t_{max} = 1/f_A$ =10 ns, so a single scan is composed by 2×10^5 points. We average 5×10^5 scans to achieve a good signal-to-noise ratio (see Fig. 6c). The transmitted probe is detected using a Thorlabs PDB430A 350 MHz balanced photo-detector and properly setting the reference line to achieve a perfect balance between the real and reference probe when the pump beam is off. The actual measuring time was $\sim$ 55 min.

5.2. Case study: ASOPS+Lock-in measurement

The $\Delta T(t)/T_0$ trace recorded with the ASOPS+Lock-in setup is shown in Fig. 6a, b (black line). We set an update rate $U_r = 200$ Hz, (*i.e.*, an integration time $t_I = 5$ ms). Therefore, to match the same number of acquisition scans with the same number of averaged pulses as that of Sec. 5.1, we set a detuning $\Delta f = 0.001$ Hz. Such choice corresponds to the same theoretical acquisition time for both ASOPS and ASOPS+Lock-in techniques, since it is determined by the number of pulses leaving the cavity. With this choice, given $f_A = 100$ MHz, each data point is given as the average over 5×10^5 probe pulses and, from the point of view of the dynamics, it encloses the information of a time delay interval $d_p = 50$ fs. As described in Sec. 5.1, the duration of the time delay window investigated in the ASOPS+Lock-in experiment is $1/f_A = 10$ ns. Thus the time-resolved trace is composed by 2×10^5 data points. In the laboratory frame, the whole measurement takes 10^3 s ($\sim$ 17 minutes) to be performed.

5.3. Case study: ECOPS+Lock-in measurement

As a third approach, we employed ECOPS+Lock-in technique. The results are displayed in Fig. 6a, b (blue curve). As in the procedure described in Sec. 5.2, we set $\Delta f = 0.001$ Hz. However, in this case, we limited the time-delay window to 500 ps, which is twenty times shorter than the 10 ns time-delay window probed in the measurements described in Sec. 5.1 and 5.2. This choice is dictated by the fact that the depletion of the beam at ν_2 ends within $\sim$ps (ideally, we could have further limited the extent of the time-delay window). The number of (pump-probe pulse) pairs needed to span a time-delay interval of 500 ps is 5×10^9. In the laboratory frame, this means that a whole trace is recorded in 50 s. At this point, we switch the detuning to $-|\Delta f|$ and we acquire a new scan of 500 ps in the opposite direction and so on. Since we employ 500 ps to perform each measurements scan only 500 ps in each measurement, in the same time window of 10 ns with this technique we can take 20 scans and we can average them. The result (restricted over the first 40 ps) is shown as a blue line in Fig. 6a. In the laboratory frame, the whole measurement takes $\sim$ 17 minutes to be performed.

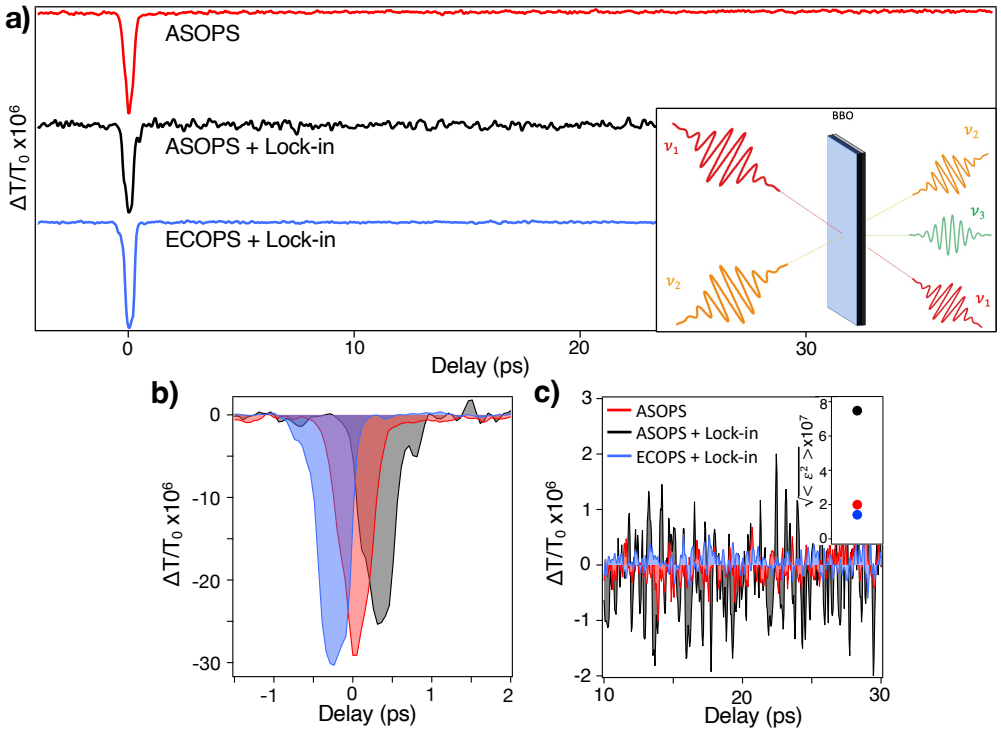

Fig. 6. Beam-depletion occurring in Sum Frequency Generation (SFG) in type I BBO crystal investigated with three approaches: ASOPS (red curve), ASOPS+Lock-in (black curve), and ECOPS+Lock-in (blue curve). a) Depletion $\Delta T(t)/T_0$ of the $\nu_2 = 384.4$ THz beam. The temporal dynamics is reported over the firsts 40 ps. The inset shows the architecture of the SFG process. b) Zoom of the $\Delta T(t)/T_0$ trace near the temporal coincidence. For clarity the traces have been slightly shifted in the horizontal direction. The sum-frequency signal temporal duration (FWHM) are 261 ± 3 fs, 273 ± 6 fs and 251 ± 6 fs for ASOPS, ASOPS+Lock-in and ECOPS+Lock-in, respectively c) Level of noise with the three noise level techniques evaluated in the delay time range from 10 ps to 30 ps. The inset report the standard deviation $\sqrt{\langle \varepsilon^2 \rangle_w}$ for each technique.

5.4. Discussion

In Fig. 6a, we show the beam depletion of the $\nu_2 = 384.4$ THz laser pulse during sum frequency generation in a type I BBO crystal as a function of the time-delay. The three traces are obtained using ASOPS (red line), ASOPS+Lock-in (black line), and ECOPS+Lock-in (blue line). In the measurements performed with the three approaches, the energy density values of the laser beams are the same. For clarity, we display the data over the first 40 ps delay time. Fig. 6b shows a zoom on the ps scale, where the relevant dynamics occurs. The three profiles are shifted along the time-delay axis (horizontal axis), for sake of visualization, to highlight that the beam depletion measured by the three techniques is the same. This assures that the physical output from the three different techniques is consistent.

Fig. 6c displays the $\Delta T(t)/T_0$ curves in the time delay interval, w, between 10 ps and 30 ps. Since the average value of each trace is zero over this range, $\langle \Delta T/T_0 \rangle_w = 0$, each trace is representative of the noise, its level being here quantified as $\delta\varepsilon = \Delta T/T_0 - \langle \Delta T/T_0 \rangle_w$. As detailed in Secs.5.1 and 5.2, the settings adopted in the ASOPS and ASOPS+Lock-in measurements are such that the theoretical time of measurement is the same, thus the number of probe pulses leaving

Table 2. Summary of control parameters as a function of laser repetition rate f_A, cavities detuning Δf, Lock-in integration time t_I, ECOPS sweep period T_{sweep}.

	ASOPS	ASOPS+Lock-in	ECOPS+Lock-in
Time delay step	$\Delta t = \Delta f / f_A^2$	$d_p = t_I \cdot \lvert\Delta f\rvert / f_A$	
Max delay time	$1/f_A$		$(T_{sweep}/2)(\lvert\Delta f\rvert/f_A)$
N_{bp}	N.A.	$t_I \cdot f_A$	

the cavity is the same (namely, 5×10^5). A detailed comparison of the noise levels would be quite involved in the present case, the noise level being biased by the use of different connecting cables/electronics equipment within the three exploited setups. That said, Fig. 6c and inset show that the noise level is within the same order of magnitude for the case of ASOPS, variance $\sqrt{\langle \delta\varepsilon^2 \rangle_w} = 2.0 \times 10^{-7}$, and ASOPS + Lock-in, $\sqrt{\langle \delta\varepsilon^2 \rangle_w} = 7.48 \times 10^{-7}$. The smaller noise level is achieved with ECOPS+Lock-in technique ($\sqrt{\langle \delta\varepsilon^2 \rangle_w} = 1.41 \times 10^{-7}$). The ECOPS+Lock-in probed a time delay window of extending at 500 ps, which is 20 times shorter than that probed with ASOPS and ASOPS+Lock-in, resulting in a total number of scans 20 times larger than recorded with ASOPS. We point out that in the ASOPS+Lock-in technique the number of averaged pulses reaching the sample is halved due to the presence of the chopper, thus the achievable signal-to-noise ratio is $\sqrt{2}$ smaller than for the ASOPS technique.

In certain instances, the time of measurement is an important factor. From a fundamental stand point, when the number of averaged probe pulses leaving the cavity and time resolution are the same for ASOPS and ASOPS+Lock-in, the time of measurements should in principle be the same, but the actual number of pulses for the ASOPS+Lock-in technique is halved by the presence of the chopper. In the present real case scenario, instead, the actual time of measurement with the ASOPS technique is almost three times longer than the one for the ASOPS+Lock-in. Although the precise measurement times are specific to the instruments here adopted, this fact highlights the advantage of using the highly developed, firmly established Lock-in technology rather than the combination of fast balanced amplified photodiodes and fast acquisition board instead. Indeed, in theoretically the ASOPS technique should be faster at constant number of pulses reaching the sample. However, the presence of dead-time due to the acquisition hardware significantly increases the actual measurement time of the ASOPS technique. In conclusion, the ECOPS+Lock-in technique performs the best also in terms of acquisition time. Indeed, the possibility to tailor the delay window as needed allows to collect more scans in less time. In the case study here discussed, we averaged 20 measurements scans (with the same settings used for the ASOPS+Lock-in case) in $\sim$ 17 minutes, yet obtaining the smaller noise level.

6. Technique at work: mechanical nanometrology

We now implement the ECOPS+Lock-in technique to inspect, via single-nanoparticle time-resolved optical microscopy, the vibrational eigenmodes of a single Au nanodisk, 100 nm thick and 250 nm in diameter, nanopaterned on a sapphire substrate, see Fig. 7a. These scenario is particularly appropriate to test the scheme since it involves accessing long-delay times in a nanoscopy setup. The ECOPS is well suited since the nano-object oscillations are damped on a timescale $\sim$ 1 ns, *i.e.*, one tenth of the delay time window explored by the employed ASOPS system. The case study is thus paradigmatic of situations where the approach is particularly apt.

Pump (1560 nm wavelength) and probe (780 nm wavelength) beams are collinearly tightly focused on a single nanodisk via a high numerical aperture (NA) objective. The transmitted beams are collected via a collecting objective identical to the focusing one. We use a Nikon

MU20500 (50X, 0.6 NA, working distance=11 mm) microscope objective to focus the pump and probe beam to FWHM diameters of 1460 nm and 730 nm, respectively. These are measured with an adapted version of the "knife-edge technique", *i.e.* by raster scanning the nanodisk across the beam and acquiring the transmission map, see Fig. 7c for the probe case. The pump pulse energy is kept at a minimum with a single pulse fluence ~ 0.1 mJ/cm^2. The intensity of the transmitted probe is measured by a single slow silicon photo-detector (Thorlabs DET210) whose output is fed to a Lock-in amplifier (Ametetek Signal Recovery DSP 7265). We employ a chopper frequency of 2947 Hz. We measured the normalized transmittivity variation $\Delta T(t)/T_0$ of a single gold nanodisk over a time-delay window of 1.5 ns adopting the ECOPS+Lock-in scheme. Here, we average 10 scans, with $f_A = 100$ MHz, $\Delta f = 0.02$ Hz, $t_I = 5$ ms and $T_{sweep} = 15$ s. These parameters imply a theoretical time of measurement of 150 s.

The trace $\Delta T/T_0$ versus delay time is reported in Fig. 7d top panel. A fast peak, due to electronic excitation, is followed by a slower relaxation background, encoding information on the electron-phonon thermalization within the Au disk and, on longer time scales, heat transfer from the disk to the substrate and within the substrate [25]. Oscillations, corresponding to the mechanical vibrations of the system, are superposed on the relaxation background. For the sake of extracting the oscillating signal, the relaxation background was first fitted with a sum of two decaying exponential functions. The relaxation background was then subtracted from the total signal to obtain the residue (red curve in Fig. 7d, bottom panel) revealing an oscillating signal lasting up to the nanosecond time scale. The residue (red line) is well fitted with a damped oscillating profile (blue line) $f(t) = A_0 \cdot e^{-\gamma t} \cdot \sin(2\pi\nu_{osc}t + \phi)$, where A_0 is the amplitude, γ is the decay parameter, ν_{osc} is the frequency and ϕ is the phase of the oscillation, see Fig. 7d bottom. The value of the frequency (period) obtained from the fit is $\nu_{osc} = 7.8$ GHz ($T_{osc} = 2\pi/\nu_{osc} = 127$ ps) and the lifetime $1/\gamma = 206$ ps. The oscillation frequency matches the breathing mode of the sapphire supported-Au nanodisk. This claim is supported by a frequency sweep analysis of the normalized mechaincal energy stored within the nanodisk excited by an external isotropic stress periodic in time, with a frequency ν, see Fig. 7e. The theoretical resonant frequency well matches the experimental one, as suggested by the spectrum obtained by Fourier transforming the time-resolved data (Fig. 7d inset). The mechanical eigenmodes and their lifetimes are key elements to access both the nanodisk morphology and mechanical adhesion to the substrate [26, 30].

This example demonstrates that the ECOPS+Lock-in approach is well suited for mechanical nanometrology of mesoscopic samples. The actual measurement time falls short of 3 minutes, thus sensibly reducing the acquisition time of traditional delay-line and ASOPS-based measurements performed on similar nano-systems [56]. We emphasize that a shorter measurement time also minimizes the sample spatial drift which is a known source of errors in time-resolved mechanical nanometrology.

7. Conclusions and perspectives

We critically reviewed the standard pump-probe techniques based either on: (a) mechanical delay stage and Lock-in detection or (b) Asynchronous Optical Sampling/Electronically Controlled Optical Sampling together with fast balanced photodiodes. We then proposed a new pump-probe scheme merging ASOPS/ECOPS with use of a single slow photodiode and Lock-in detection. This approach unites the pros of the traditional schemes and reduces the layout complexity. As a proof of concept benchmark experiment, we adopted the three approaches (ASOPS, ASOPS+Lock-in, and ECOPS+Lock-in) to investigate beam-depletion process occurring in sum frequency generation in a type I BBO crystal. Results show that the ECOPS+Lock-in technique is a viable alternative to the other approaches, well performing in terms of acquisition time, S/N and lay-out simplicity, while adopting wide spread, off-of-the shelve instrumentation. We then exploited the proposed ECOPS+Lock-in scheme to characterize, via optical time-resolved

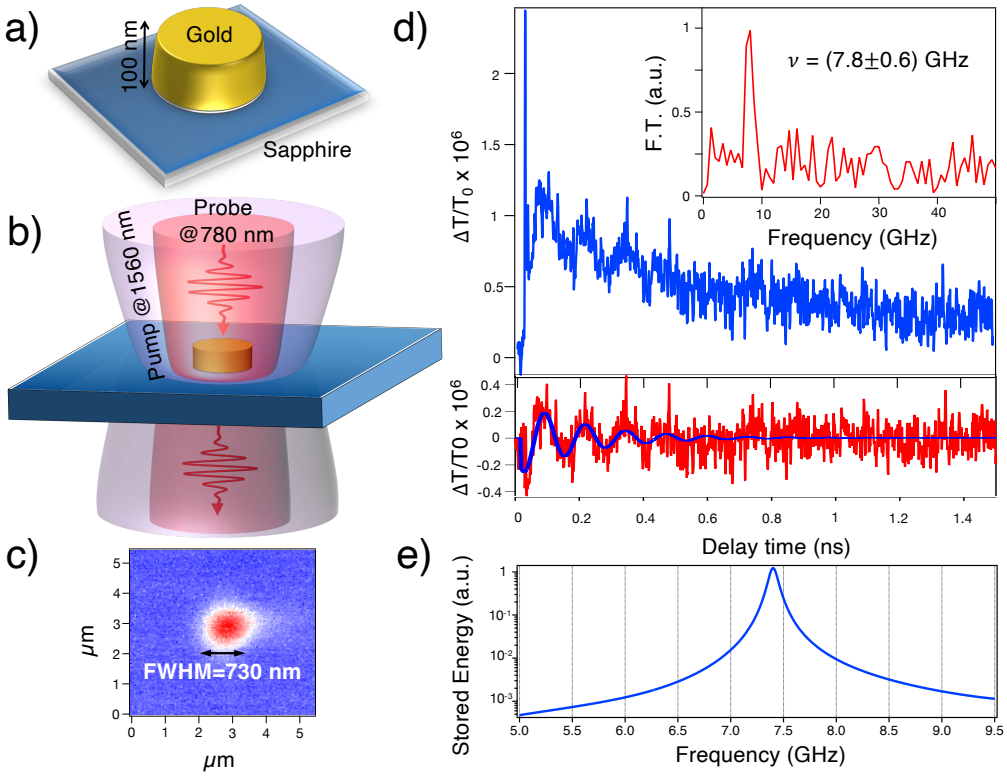

Fig. 7. a) Sample. Gold nanodisk: 100 nm height and 250 nm diameter nanopatterned on a sapphire substrate. b) Pump (1560 nm) and probe (780 nm) beams collinearly focused on the nanodisk. c) Image of the probe beam intensity at its waist obtained raster scanning the beam waist plane with the Au nanodisk. FWHM of the beam intensity profile at the nanodisk plane: 730 nm for the probe, 1460 nm for the pump (not shown). d) (Top panel) relative transmittivity variation $\Delta T(t)/T_0$ of the probe beam as a function of the delay between pump and probe, t. (Bottom panel) Residuals (red trace) obtained by subtracting the "thermal background" from the experimental $\Delta T(t)/T_0$ curve shown in top panel d (see details in the text). Blue curve: fit to the residual. The oscillation period is T_{osc} = 127 ps. Inset: Modulus of the Fourier Transform of the residual. e) Normalized mechanical energy stored in the nanodisk as a function of the frequency of the external stress applied to the nanodisk itself, calculated by finite element simulations.

microscopy, the mechanics of a single gold nanodisk nanopatterned on a sapphire substrate. We achieved high spatial stability, due to the absence of moving parts, and short acquisition times. This demonstration proofs the ECOPS+Lock-in scheme as particularly suited in mechanical nanometrology applications in an industrial setting.

In perspective, the proposed scheme can be further simplified adopting a single-cavity dual-comb laser system [57–59] instead of two synchronized laser cavities , single laser diode-based ASOPS [60] and optical sampling by repetition-rate tuning [61, 62] techniques. Reducing setup costs and complexity would have a dual benefit: not only would it make the system more affordable, but it would also minimize the risk of failure, resulting in a more reliable and durable system.

Funding. Content in the funding section will be generated entirely from details submitted to Prism.

Acknowledgments. A. Tognazzi and M. Gandolfi thanks for the financial support the European Union through "FESR o FSE, PON Ricerca e Innovazione 2014-2020 - DM 1062/2021".

Disclosures. The authors declare no conflicts of interest.

Data Availability Statement. All data in support of the findings of this paper are available within the article or as supplementary material.

Supplemental document. No supplemental document available.

References

1. E. A. A. Pogna, M. Celebrano, A. Mazzanti, *et al.*, "Ultrafast, all optically reconfigurable, nonlinear nanoantenna," ACS Nano **15**, 11150–11157 (2021).
2. Y. Hu, M. Tong, S. Hu, *et al.*, "Multidimensional engineered metasurface for ultrafast terahertz switching at frequency-agile channels," Nanophotonics **11**, 1367–1378 (2022).
3. A. Mazzanti, E. A. A. Pogna, L. Ghirardini, *et al.*, "All-optical modulation with dielectric nanoantennas: Multiresonant control and ultrafast spatial inhomogeneities," Small Sci. **1**, 2000079 (2021).
4. B. Li, R. Camacho-Morales, N. Li, *et al.*, "Fundamental limits for transmission modulation in VO_2 metasurfaces," Photonics Res. **11**, B40 (2022).
5. A. Di Francescantonio, A. Locatelli, X. Wu, *et al.*, "Coherent control of the nonlinear emission of single plasmonic nanoantennas by dual-beam pumping," Adv. Opt. Mater. **10** (2022).
6. G. P. Zograf, M. I. Petrov, S. V. Makarov, and Y. S. Kivshar, "All-dielectric thermonanophotonics," Adv. Opt. Photonics **13**, 643 (2021).
7. A. Milloch, U. Filippi, P. Franceschini, *et al.*, "Halide perovskite artificial solids as a new platform to simulate collective phenomena in doped mott insulators," Nano Lett. **23**, 10617–10624 (2023).
8. A. Tognazzi, P. Franceschini, O. Sergaeva, *et al.*, "Giant photoinduced reflectivity modulation of nonlocal resonances in silicon metasurfaces," Adv. Photonics **5** (2023).
9. A. O. Krushynska, D. Torrent, A. M. Aragòn, *et al.*, "Emerging topics in nanophononics and elastic, acoustic, and mechanical metamaterials: an overview," Nanophotonics **12**, 659–686 (2023).
10. D. Nardi, M. Travagliati, M. M. Murnane, *et al.*, "Impulsively excited surface phononic crystals: A route toward novel sensing schemes," IEEE Sensors J. **15**, 5142–5150 (2015).
11. D. Nardi, M. Travagliati, M. E. Siemens, *et al.*, "Probing thermomechanics at the nanoscale: Impulsively excited pseudosurface acoustic waves in hypersonic phononic crystals," Nano Lett. **11**, 4126–4133 (2011).
12. R. C. Ng, A. El Sachat, F. Cespedes, *et al.*, "Excitation and detection of acoustic phonons in nanoscale systems," Nanoscale **14**, 13428–13451 (2022).
13. K. Elsayad, F. Palombo, T. Dehoux, and D. Fioretto, "Brillouin light scattering microspectroscopy for biomedical research and applications: introduction to feature issue," Biomed. optics express **10**, 2670–2673 (2019).
14. J. Margueritat, A. Virgone-Carlotta, S. Monnier, *et al.*, "High-frequency mechanical properties of tumors measured by brillouin light scattering," Phys. review letters **122**, 018101 (2019).
15. M. Abi Ghanem, T. Dehoux, O. F. Zouani, *et al.*, "Remote opto-acoustic probing of single-cell adhesion on metallic surfaces," J. Biophotonics **7**, 453–459 (2014).
16. C. Glorieux, "Perspective on non-invasive and non-destructive photoacoustic and photothermal applications," J. Appl. Phys. **131**, 170903 (2022).
17. O. Matsuda and O. B. Wright, "Picosecond laser ultrasonics," Ultrasonics **56**, 3–20 (2015).
18. T. Thréard, E. de Lima Savi, S. Avanesyan, *et al.*, "Photoacoustic 3-d imaging of polycrystalline microstructure improved with transverse acoustic waves," Photoacoustics **23**, 100286 (2021).
19. B. Abad, J. L. Knobloch, T. D. Frazer, *et al.*, "Nondestructive measurements of the mechanical and structural properties of nanostructured metalattices," Nano letters **20**, 3306–3312 (2020).
20. D. Brick, E. Emre, M. Grossmann, *et al.*, "Picosecond photoacoustic metrology of SiO_2 and $LiNbO_3$ layer systems used for high frequency surface-acoustic-wave filters," Appl. Sci. **7** (2017).
21. S. Peli, N. Nembrini, F. Damin, *et al.*, "Discrimination of molecular thin films by surface-sensitive time-resolved optical spectroscopy," Appl. Phys. Lett. **107**, 163107 (2015).
22. S. Peli, E. Cavaliere, G. Benetti, *et al.*, "Mechanical properties of Ag nanoparticle thin films synthesized by supersonic cluster beam deposition," The J. Phys. Chem. C **120**, 4673–4681 (2016).
23. T. Stoll, P. Maioli, A. Crut, *et al.*, "Time-resolved investigations of the cooling dynamics of metal nanoparticles: Impact of environment," The J. Phys. Chem. C **119**, 12757–12764 (2015).
24. A. Crut, P. Maioli, N. D. Fatti, and F. Vallée, "Acoustic vibrations of metal nano-objects: Time-domain investigations," Phys. Reports **549**, 1 – 43 (2015). Acoustic vibrations of metal nano-objects: Time-domain investigations.
25. M. Gandolfi, A. Crut, F. Medeghini, *et al.*, "Ultrafast thermo-optical dynamics of plasmonic nanoparticles," The J. Phys. Chem. C **122**, 8655–8666 (2018).
26. W.-S. Chang, F. Wen, D. Chakraborty, *et al.*, "Tuning the acoustic frequency of a gold nanodisk through its adhesion layer," Nat. Commun. **6**, 7022 EP – (2015). Article.
27. R. Fuentes-Domínguez, S. Naznin, L. Marques, *et al.*, "Characterising the size and shape of metallic nano-structures by their acoustic vibrations," Nanoscale **12**, 14230–14236 (2020).

28. A. M. Weiner, *Ultrafast Optics* (John Wiley & Sons, Inc., 2009).
29. J. H. Scofield, "Frequency-domain description of a lock-in amplifier," Am. J. Phys. **62**, 129–133 (1994).
30. F. Medeghini, R. Rouxel, A. Crut, *et al.*, "Signatures of small morphological anisotropies in the plasmonic and vibrational responses of individual nano-objects," The J. Phys. Chem. Lett. **10**, 5372–5380 (2019).
31. T. Hochrein, R. Wilk, M. Mei, *et al.*, "Optical sampling by laser cavity tuning," Opt. Express **18**, 1613 (2010).
32. N. Krauß, A. Nast, D. C. Heinecke, *et al.*, "Fiber-coupled high-speed asynchronous optical sampling with sub-50 fs time resolution," Opt. Express **23**, 2145–2156 (2015).
33. Y. L. Duan L, "Ultrafast optical sampling finds applications in precision measurement," J. Sci. Ind. Metrol. **1**, 5 (2016).
34. Z. Wu, A. Li, R. Xue, *et al.*, "High-precision surface profilometry on a micron-groove based on dual-comb electronically controlled optical sampling," Appl. Opt. **62**, 8793 (2023).
35. A. Bartels, R. Cerna, C. Kistner, *et al.*, "Ultrafast time-domain spectroscopy based on high-speed asynchronous optical sampling," Rev. Sci. Instruments **78**, 035107 (2007).
36. F. Pérez-Cota, R. J. Smith, E. Moradi, *et al.*, "Thin-film optoacoustic transducers for subcellular Brillouin oscillation imaging of individual biological cells," Appl. Opt. **54**, 8388–8398 (2015).
37. F. Pérez-Cota, R. J. Smith, E. Moradi, *et al.*, "High resolution 3D imaging of living cells with sub-optical wavelength phonons," Sci. Reports **6**, 39326 EP – (2016). Article.
38. T. Dehoux, M. A. Ghanem, O. F. Zouani, *et al.*, "All-optical broadband ultrasonography of single cells," Sci. Reports **5**, 8650 EP – (2015). Article.
39. R. J. Smith, F. P. Cota, L. Marques, *et al.*, "Optically excited nanoscale ultrasonic transducers," The J. Acoust. Soc. Am. **137**, 219–227 (2015).
40. F. Noll, N. Krauß, V. Gusev, *et al.*, "Surface plasmon-based detection for picosecond ultrasonics in planar gold-dielectric layer geometries," Photoacoustics **30**, 100464 (2023).
41. S. Peli, E. Cavaliere, G. Benetti, *et al.*, "Mechanical properties of Ag nanoparticle thin films synthesized by supersonic cluster beam deposition," The J. Phys. Chem. C **120**, 4673–4681 (2016).
42. P. O. Vaccaro, M. Alonso, M. Garriga, *et al.*, "Localized thinning for strain concentration in suspended germanium membranes and optical method for precise thickness measurement," AIP advances **8**, 115131 (2018).
43. D. Brick, M. Hofstetter, P. Stritt, *et al.*, "Glass transition of nanometric polymer films probed by picosecond ultrasonics," Ultrasonics **119**, 106630 (2022).
44. M. Travagliati, D. Nardi, C. Giannetti, *et al.*, "Interface nano-confined acoustic waves in polymeric surface phononic crystals," Appl. Phys. Lett. **106**, 021906 (2015).
45. J. D. Greener, E. de Lima Savi, A. V. Akimov, *et al.*, "High-frequency elastic coupling at the interface of van der waals nanolayers imaged by picosecond ultrasonics," ACS nano **13**, 11530–11537 (2019).
46. M. R. Wagner, B. Graczykowski, J. S. Reparaz, *et al.*, "Two-dimensional phononic crystals: Disorder matters," Nano Lett. **16**, 5661–5668 (2016). PMID: 27580163.
47. D. Nardi, M. Travagliati, M. M. Murnane, *et al.*, "Impulsively excited surface phononic crystals: A route toward novel sensing schemes," IEEE Sensors J. **15**, 5142–5150 (2015).
48. M. Gandolfi, S. Peli, M. Diego, *et al.*, "Ultrafast photoacoustic nanometrology of InAs nanowires mechanical properties," The J. Phys. Chem. C **126**, 6361–6372 (2022).
49. T. Yasui, Y. Kabetani, Y. Ohgi, *et al.*, "Absolute distance measurement of optically rough objects using asynchronous-optical-sampling terahertz impulse ranging," Appl. Opt. **49**, 5262 (2010).
50. P. A. Elzinga, R. J. Kneisler, F. E. Lytle, *et al.*, "Pump/probe method for fast analysis of visible spectral signatures utilizing asynchronous optical sampling," Appl. Opt. **26**, 4303 (1987).
51. V. A. Stoica, Y.-M. Sheu, D. A. Reis, and R. Clarke, "Wideband detection of transient solid-state dynamics using ultrafast fiber lasers and asynchronous optical sampling," Opt. Express **16**, 2322–2335 (2008).
52. A. Nagakubo, K. Kanai, H. Tamura, *et al.*, "Variable repetition frequency asynchronous optical sampling method without a feedback loop," AIP Adv. **12** (2022).
53. M. C. Velsink, M. Illienko, P. Sudera, and S. Witte, "Optimizing pump–probe reflectivity measurements of ultrafast photoacoustics with modulated asynchronous optical sampling," Rev. Sci. Instruments **94** (2023).
54. T. Yasui, E. Saneyoshi, and T. Araki, "Asynchronous optical sampling terahertz time-domain spectroscopy for ultrahigh spectral resolution and rapid data acquisition," Appl. Phys. Lett. **87** (2005).
55. R. W. Boyd, *Nonlinear optics* (Academic Press, 2008).
56. A. Ronchi, P. Franceschini, A. D. Poli, *et al.*, "Nanoscale self-organization and metastable non-thermal metallicity in Mott insulators," Nat. Commun. **13** (2022).
57. J. Pupeikis, B. Willenberg, F. Bruno, *et al.*, "Picosecond ultrasonics with a free-running dual-comb laser," Opt. Express **29**, 35735 (2021).
58. J. Pupeikis, B. Willenberg, S. L. Camenzind, *et al.*, "Spatially multiplexed single-cavity dual-comb laser," Optica **9**, 713 (2022).
59. J. Pupeikis, W. Hu, B. Willenberg, *et al.*, "Efficient pump-probe sampling with a single-cavity dual-comb laser: Application in ultrafast photoacoustics," Photoacoustics **29**, 100439 (2023).
60. I. Ejidike, R. A. McCracken, and D. Bajek, "Modelling two-laser asynchronous optical sampling using a single 2-section semiconductor mode-locked laser diode," Opt. Express **30**, 3289 (2022).
61. D. Bajek and M. A. Cataluna, "Megahertz scan rates enabled by optical sampling by repetition-rate tuning," Sci.

Reports **11** (2021).
62. D. Bajek and M. A. Cataluna, "Fast optical sampling by electronic repetition-rate tuning using a single mode-locked laser diode," Opt. Express **29**, 6890 (2021).